sciendo
ISSN 1335-8871
MEASUREMENT SCIENCE REVIEW
Journal homepage: https://content.sciendo.com

DEEP-BTS: Deep Learning based Brain Tissue Segmentation using ResU-Net Model

Sivaprakash P[1*], Banumathi J[2], Ashis Kumar Mishra[3], Jayapriya P[4]

[1]*Department of Computer Science and Engineering (AI & ML), Rathinam Technical Campus, Eachanari, Coimbatore, Tamil Nadu, 641021, India, sivaprakashcse0402@gmail.com*
[2]*Department of Computer Science and Engineering, University College of Engineering, Nagercoil, Tamil Nadu, 629004, India, banumathi@ucen.ac.in*
[3]*School of Computer Sciences, Odisha University of Technology and Research (OUTR), Bhubaneswar, Odisha, 751029, India, akmishracse@outr.ac.in*
4Department of Computer Science and Engineering, Dr. N.G.P Institute of Technology, Coimbatore, Tamil Nadu, 641048, India, jayapriy@gmail.com

Abstract: Brain tissue segmentation (BTS) in MRI is essential for diagnosing neurological disorders, mapping brain structures, and analyzing disease progression. A major challenge in BTS is intensity inhomogeneity, where non-uniform illumination in MRI scans causes intensity variations, making it difficult to accurately differentiate gray matter (GM), cerebrospinal fluid (CSF), and white matter (WM). To address these challenges, a novel deep learning-based DEEP-BTS model has been proposed for BTS with brain MRI images. The input images are collected from the BrainWeb dataset, where MRI images undergo skull stripping to remove unnecessary regions. After skull stripping, the collected images are pre-processed using a contrast stretching adaptive trilateral filter (CSATF) to improve image quality, reduce noise artifacts, and perform augmentation to increase data diversity to ensure robust model training. The pre-processed images are then fed into the ResU-Net, which segments different brain tissues, including CSF, GM, and WM. The proposed DEEP-BTS model is evaluated based on its accuracy (*AC*), specificity (*SP*), recall (*RE*), precision (*PR*), F1 score (*F*1), Jaccard index (*JI*), and Dice index (*DI*). The proposed DEEP-BTS achieved a segmentation accuracy of 98.91 % for BTS. The proposed ResU-Net outperformed Fuzzy C-Means, M-Net, and U-Net methods, achieving 98.33 % CSF, 98.04 % GM, and 99.15 % WM, indicating improved segmentation accuracy.

Keywords: brain tissue segmentation, contrast stretching adaptive trilateral filter, cerebrospinal fluid, gray matter, white matter

1. INTRODUCTION

The human brain, often observed as the epicenter of nervous activity, is one of the body's most vital yet intricate organs [1], [2]. A tumor is a collection of abnormal swelling of brain cells in the nervous system [3]. High-resolution brain images with a range of contrasts can be obtained using MRI, a non-invasive and safe imaging technique [4], [5]. Its abilities have led to its widespread use in diagnosing neurological conditions. There is interest in assessing how the brains of infants and adults develop, as MRI provides a powerful non-invasive technique for studying brain anatomy and function [6], [7]. This interest arises because MRI produces several cross-sectional images with varying contrasts, enabling safe and non-invasive investigation of the brain [8]. Brain image segmentation is crucial for both basic neuroscience research and clinical diagnosis to evaluate neurological disorders [9], [10]. Given a brain image, usually obtained by MRI, brain image segmentation estimates an annotated (labeled) image. This image is divided into multiple anatomical/structural regions, and the set for each voxel is created beforehand [11]. Instead of relying on specialists' visual inspection, segmentation allows for objective diagnosis and study by providing a quantitative assessment of brain tissue volume [12].

The accuracy and processing efficiency of deep learning (DL)-based automatic segmentation techniques are significantly higher than those of conventional techniques [13]. By precisely identifying brain regions of interest and distinguishing them from healthy brain tissue, DL techniques enable more precise quantitative analysis [14]. Many clinical and neurological studies depend on the segmentation of the brain's gray matter (GM), white matter (WM), and cerebrospinal fluid (CSF) [15]. This DL-based segmentation supports image-guided procedures, makes surgical planning

DOI: 10.2478/mr-2025-0041
Corresponding author: banumathi@ucen.ac.in (Banumathi J)

easier, and allows for the visualization and investigation of anatomical components [16], [17]. Additionally, DL-based techniques have made significant progress in segmenting brain tissue, including that of adults, newborns, and fetuses [18]. Segmenting brain MRI is challenging due to complex structures and intensity variations. Accurate segmentation of patients using MRI remains difficult for more effective diagnosis and treatment. Furthermore, automatic segmentation is challenging because of the complexity and diversity of brain tissues. In this paper, a novel DL-based DEEP-BTS model is proposed for brain tissue segmentation (BTS) with brain MRI. The contributions of this work are summarized as follows:

- The first step is skull stripping, which removes the skull and scalp from the MRI images. After skull stripping, the images are enhanced using contrast stretching adaptive trilateral filter (CSATF) to improve tissue contrast and reduce noise while preserving important details.
- The noise-free images are then fed into the ResU-Net architecture. This model combines U-Net's efficient segmentation capabilities with ResNet residual connections, allowing it to learn complex features of brain tissues while maintaining accuracy.
- The ResU-Net model segments the MRI images into different brain regions, including GM, CSF, and WM.

The structure of the paper is organized as follows: Section 2 presents the literature survey; Section 3 explains the DEEP-BTS model; Section 4 provides the performance outcomes and comparative analysis; and Section 5 concludes with the conclusion and future work.

2. LITERATURE SURVEY

In recent years, researchers have proposed numerous approaches to improve the accuracy of BTS segmentation. This section summarizes recent machine learning (ML) and DL studies focused on segmenting various BTS conditions using image-based data and advanced computational techniques.

In 2024, Mohammadiet al. [19] proposed a BTS that addresses Intensity Non-Uniformity artifacts and Multiple Sclerosis lesions. Compared to previous methods for BTS and Multiple Sclerosis lesion segmentation, the proposed methodology demonstrates significant improvement in the Dice index (*DI*), particularly under high noise and artifact conditions. Experimental results show that the recommended technique outperforms FCB Former, U-Net, and Attention U-Net in terms of *DI* performance in the BTS.

In 2024, Kollem [20] introduced a technique for classifying and segmenting MRI brain tumor tissue using an optimal SVM. To achieve a sparse representation of an image's smooth contour, the contourlet transform uses a twin filter bank structure consisting of a directional filter and the Laplacian pyramid.

In 2024, Gudise et al. [21] proposed an enhanced firefly algorithm based on chaos, integrated with fuzzy C-eans (CEFAFCM), to separate tissues from brain MRIs. The Firefly Algorithm (FA) and a chaotic map are used together with a spatially modified FCM method called CEFAFCM to initialize the firefly population. Experimental results show that the proposed method outperforms several existing brain MRI segmentation techniques, including FCM, BCFCM, FAFCM, and En-FAFCM.

In 2024, Daoudi and Mahmoudi [22] proposed WM, GM, and CSF tissue classifications for MR brain imaging. To improve treatment accuracy, the proposed segmentation procedure combines two algorithms: Whale Optimization Algorithm (WOA) and the Hidden Markov Random Field (HMRF).

In 2021, Veluchamy and Subramani [23] proposed a segmentation method for brain tissue in a medical decision support system. Quantitative parameters such as peak signal-to-noise ratio (*PSNR*), discrete entropy, specificity (*SP*), F1 score (*F*1), accuracy (*AC*), Jaccard index (*JI*), and *DI* are used to compare the proposed approach with other current approaches. Experiments indicate that the proposed technique achieves a reasonable balance between noise and intensity inhomogeneity.

In 2020, Yamanakkanavar and Lee [24] proposed a patch-wise M-net to automatically segment MRI images of the brain. According to experimental data, the proposed approach outperformed state-of-the-art methods, achieving average segmentation accuracy of 95.44 % for GM, 94.81 % for CS, and 96.33 % for WM.

In 2021, Long et al. [25] introduced a Multi-Scale Learning U-Net Based Encoding-Decoding Method for BTS in MRI. The study also developed a multi-branch output structure that generates more precise, edge-preserving forecasting maps by combining dense neighboring prediction features at dissimilar scales during the decoding stage.

In 2023, Karimi et al. [26] proposed a U-Net for learning to separate the fetal brain tissue from noise annotations. The proposed techniques appropriately account for tissue boundary ambiguity. The approach produced results that were significantly more accurate than several advanced techniques, with U-Net being the closest competitor.

From this literature, existing techniques for BTS using various ML and DL models exhibit several limitations. One major challenge in BTS is the intensity of homogeneity caused by MRI artifacts. This leads to non-uniform brightness across the image, making it difficult to distinguish between different tissue types. Traditional thresholding or clustering methods struggle with this variation, reducing segmentation accuracy. Additionally, the presence of noise and partial volume effects further complicates boundary detection. To address these problems, a novel DEEP-BTS method was introduced for the accurate classification of BTS.

3. PROPOSED DEEP-BTS

In this research, a novel DL-based DEEP-BTS model is developed for BTS using brain MRI images. Fig. 1 shows the DEEP-BTS methodology.

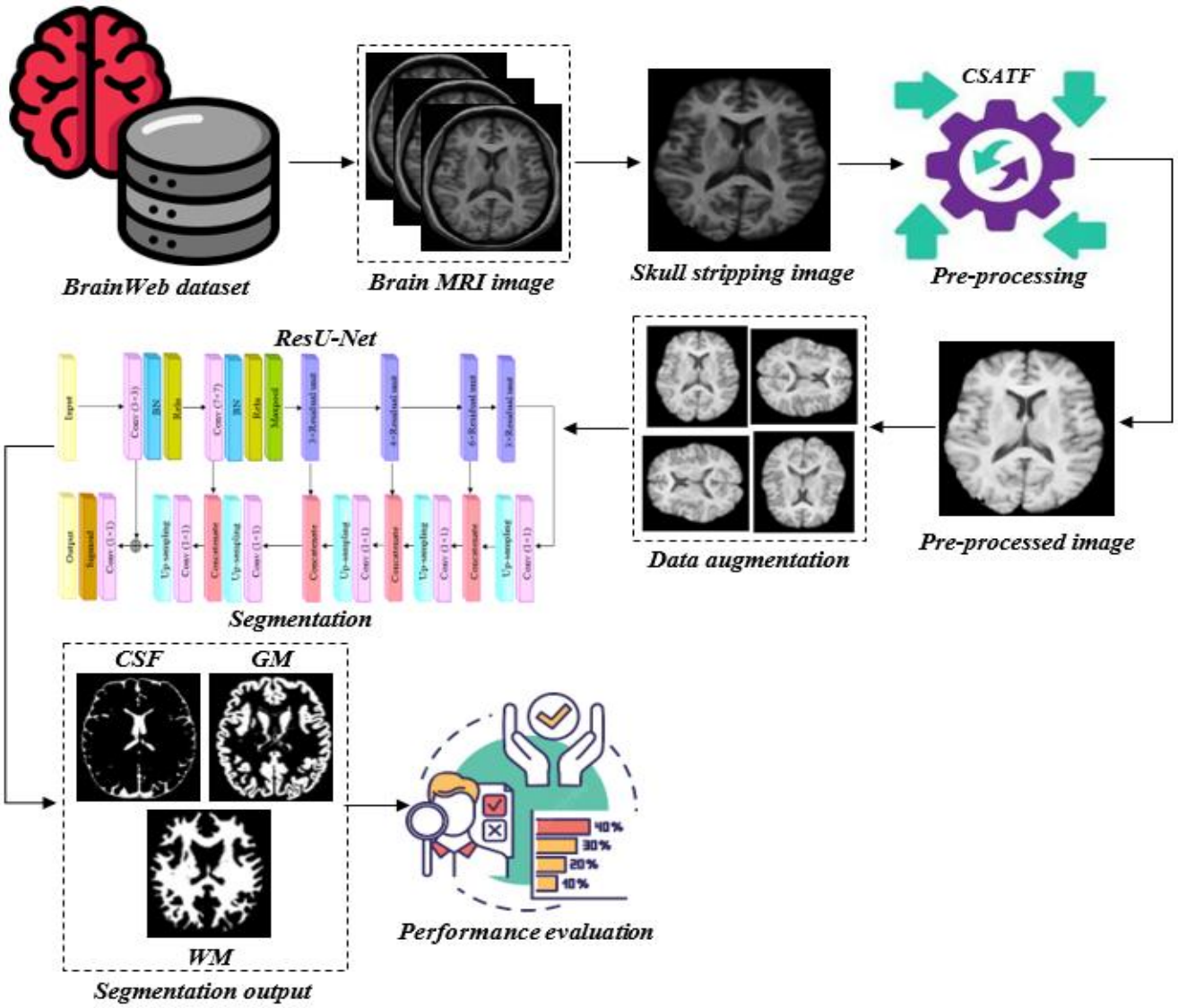

Fig. 1. Proposed DEEP-BTS methodology.

A. Dataset description

Brain MRI scans are extracted from the BrainWeb dataset. The popular synthetic MRI dataset BrainWeb offers controlled situations with varying intensity non-uniformities (RF inhomogeneities) and noise levels. Key characteristics include RF inhomogeneity levels of 0 %, 20 %, and 40 %, which simulate intensity non-uniformities, and noise levels of 0 %, 1 %, 3 %, and 5 %. The training set contains 36 images from all noise and RF levels, the validation set contains 12 images, and the test set contains 57 images.

B. Pre-processing

In pre-processing to enhance the quality of MRI images, skull stripping is performed first. After stripping the skull from the input MRI image, the MRI image is pre-processed using CSATF. CSATF combines two filters: contrast stretching (CS) and adaptive trilateral (AT) filter.

Contrast stretching:

In this denoising phase, each original intensity value is replaced, and histogram comparisons are conducted using a locally modified contrast-stretching adjustment. A new level is assigned to each pixel by applying a flexible transfer function derived from the characteristics of the MRI images.

$$Range = |Q_{\max -} Q_{\min}| \tag{1}$$

where Q is the input image, and the calculation of the strength range of the input determines the range. Here $Q_{\max}$ and $Q_{\min}$ are the maximum and minimum values of the input image for the new intensity. Each pixel is given an additional intensity using the following equations:

$$X_k = \begin{cases} Q_{N-}\sigma_N & ,if\ Q_N = Q_{\max} \\ Q_{N+}\sigma_N & ,if\ Q_N = Q_{\min} \end{cases} \tag{2}$$

$$r_n = M - \sqrt{(Range} - M)^2 \tag{3}$$

Each pixel value is altered using the given formulas, where M ranges between 0.01 and 0.02.

Adaptive trilateral filter:

The MRIs are pre-processed using the ATF to remove noise artifacts. It implements the guiding principles of the bilateral filter. The issue of high-gradient zones being ineffectively filtered by bilateral filters is resolved by using a trilateral filter under tilting. When a bilateral filter is applied to the image data, p should average highly related surrounding pixels and eliminate dissimilar pixels, yielding the tilting angle h_θ of a trilateral filter at the target pixel.

$$h_\theta(q) = \frac{1}{l_\theta}\sum_q \sum_p f_p\, e(q,p)\, z(f_q, f_p) \tag{4}$$

When the kernel is tilted, the trilateral filter's $e(.)$ and $z(.)$ functions become non-orthogonal. Equation (5) establishes the value of each pixel at this plane.

$$j(q,p) = f(q) + h_\theta.(||q-p||) \tag{5}$$

where $|q-p|$ is the multi-dimensional spacing between q and $f(q)$, represented by q at a target pixel, and h_θ is the tilting angle. To find the output of a trilateral filter, the resulting image is first passed through a bilateral filter, and then the value j is removed from the surrounding area of the target pixel.

$$f_o(q) = f_{in}(y) + t(y)\Delta \tag{6}$$

where Δ is the spatial distance between pixels q and p, and $f_o(q)$ is the output function. Tilting improves the filter's capacity to smooth high-gradient zones. It is insufficient because trilateral filter failure can still occur when tilting happens in areas with significant gradient variations. Data augmentation is an essential pre-processing technique that uses synthetic data to help the model learn and generalize features better. The ideal way to support the network's learning of the desired features is to use data augmentation. Fig. 2 shows the pre-processing stages.

C. Segmentation

The noise-free images are fed into the ResU-Net [27] model, which segments different brain tissues, including GM, CSF, and WM. To address the issue of training degradation as network layer depth increases, each convolutional (Conv) layer in the U-Net model encoding path is replaced with a residual learning block. Fig. 3 depicts the ResU-Net architecture.

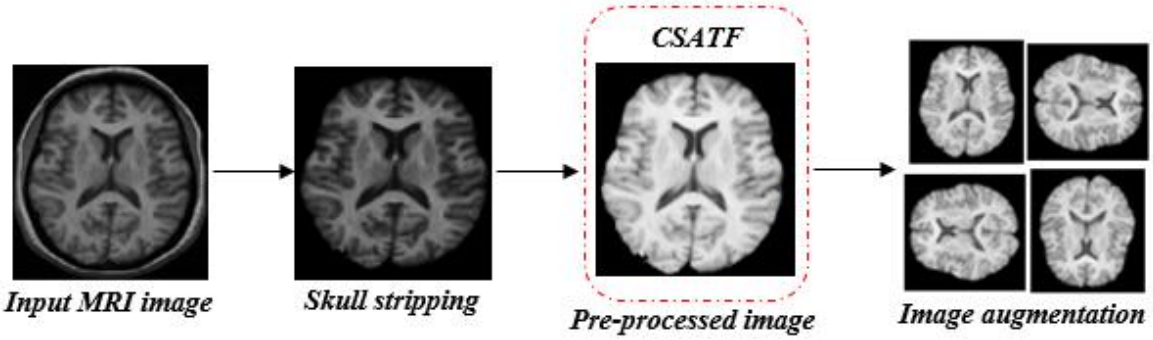

Fig. 2. Pre-processing step in the proposed method.

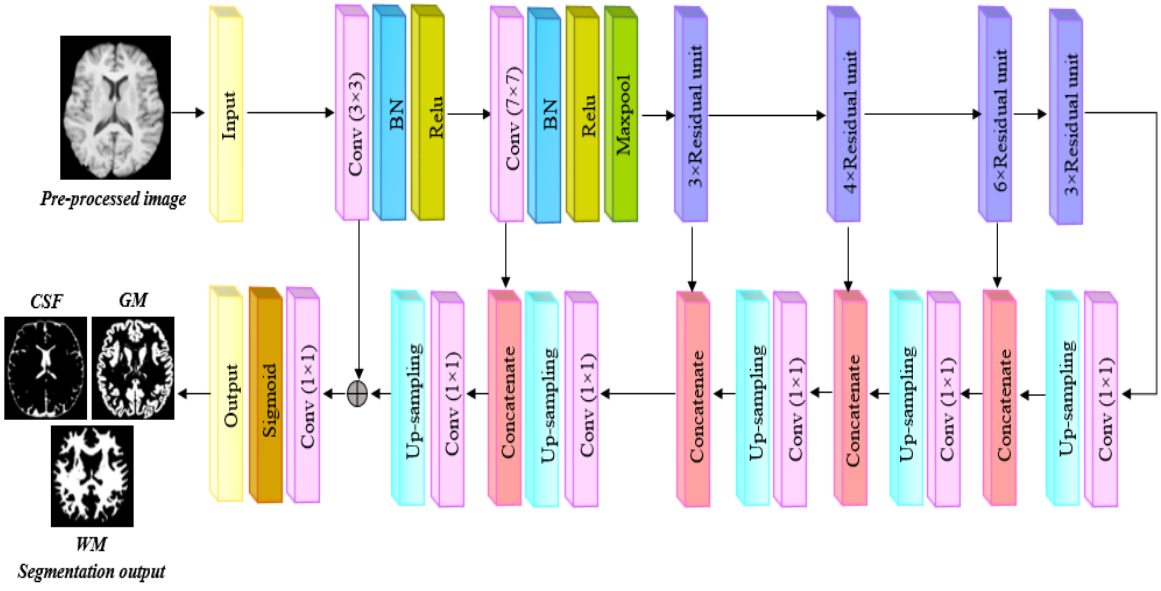

Fig. 3. Architecture of ResU-Net.

The encoding path consists of three components: an input unit, a residual unit, and a head unit. The head unit includes a BN layer and a ReLU after two conv layers. The first residual unit contains three residual blocks layered with nine conv layers. The second residual unit comprises four residual blocks layered with twelve conv layers. The third residual unit consists of six residual blocks and 18 conv layers. The fourth residual unit contains three residual blocks and nine conv layers. In this work, default parameters were used for the residual unit structures. An output unit, one addition block, and four concatenation blocks are applied repeatedly throughout the decoding path. Each concatenation block consists of a one-to-one conv and upsampling, which reduces the number of feature channels by half. Output feature maps are generated from the corresponding residual unit of the encoding path, as well as output feature maps. Segmentation results are mapped for binary classification at the last layer of the decoding path using a sigmoid activation and a 1×1 convolution filter. Between each residual block's output feature and the decoding path's conv layer, copy and crop operations are applied. Multi-scale feature fusion requires the cropping and copy operations.

4. RESULTS AND DISCUSSION

This section uses Matlab-2019b and the DL toolbox to evaluate the proposed model efficiency. The DEEP-BTS model is assessed using various measures, including *AC*, *SP*, recall (*RE*), precision (*PR)*, and *F*1. Benchmarks include the overall accuracy rates of the DEEP-BTS method, with performance explicitly specified and assessed.

Fig. 4 presents the simulation results of the proposed DEEP-BTS model using different input brain MRI image samples from the BrainWeb dataset. Column 1 displays the original brain MRI scans, while Column 2 shows the skull stripping MRI images to focus on brain tissues. Column 3 illustrates the pre-processed MRI scans for improved segmentation accuracy. Column 4 depicts variations of the MRI slices generated using augmentation techniques. Columns 5 to 7 present the segmented outputs for different brain tissues, such as CSF, WM, and GM.

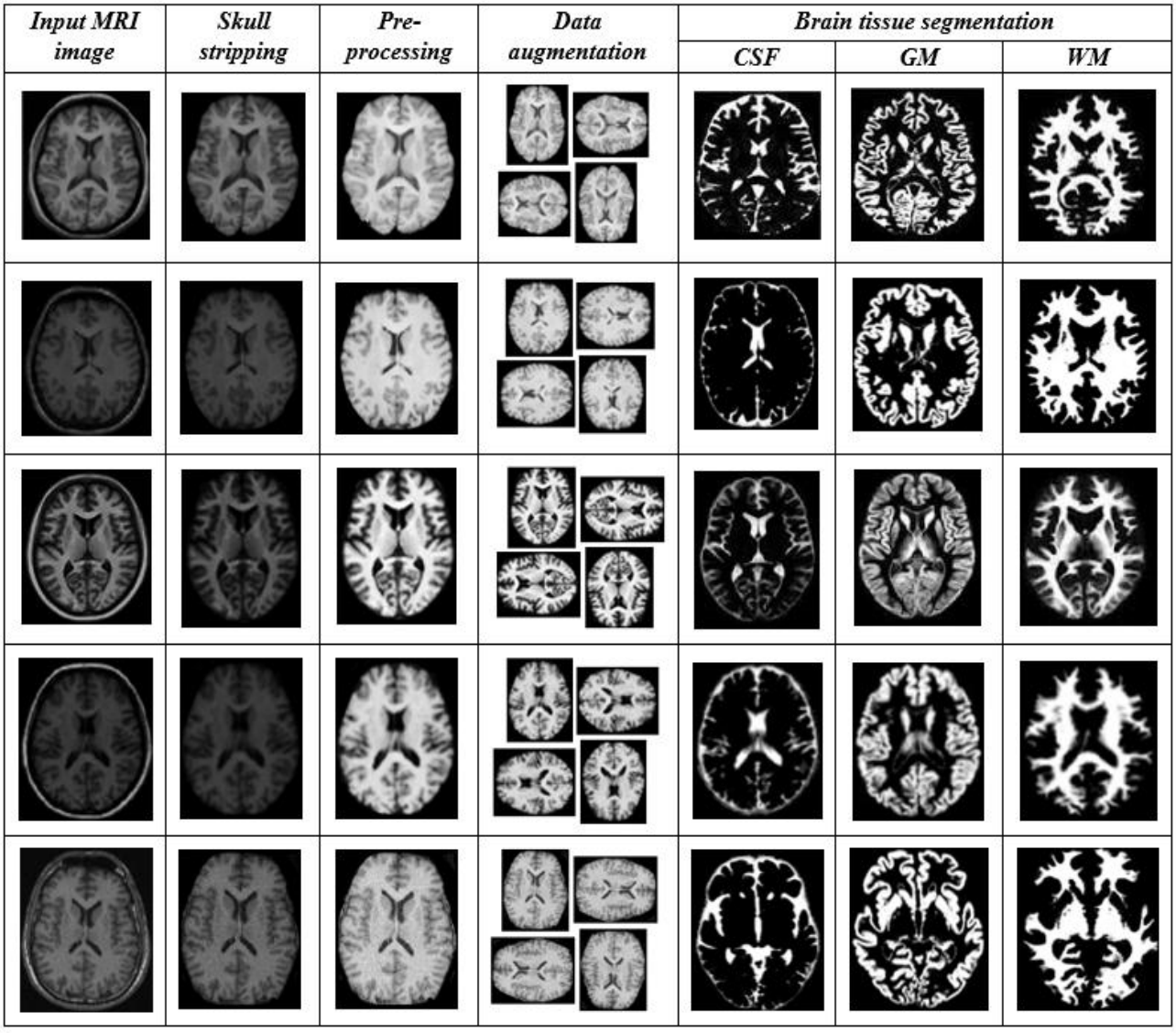

Fig. 4. Experimental results of the proposed DEEP-BTS.

A. Performance analysis

A proposed DEEP-BTS model was evaluated based on *SP*, *RE*, *PR*, *AC*, and *F1*.

$$SP = \frac{T_{\text{neg}}}{T_{\text{neg}} + F_{\text{pos}}} \tag{7}$$

$$RE = \frac{T_{\text{pos}}}{T_{\text{pos}} + F_{\text{neg}}} \tag{8}$$

$$PR = \frac{T_{\text{pos}}}{T_{\text{pos}} + F_{\text{pos}}} \tag{9}$$

$$AC = \frac{T_{\text{pos}} + T_{\text{neg}}}{Total\ no.of\ samples} \tag{10}$$

$$F1 = 2\left(\frac{PR + RE}{PR + RE}\right) \tag{11}$$

Here, T_{neg} and T_{pos} represent the true negatives and true positives of the sample images, while F_{neg} and F_{pos} represent the false negatives and false positives of the input images.

Table 1 shows the classification performance achieved by the proposed DEEP-BTS model for BTS. *AC*, *SP*, *RE*, *PR*, and *F*1 are the metrics used to determine performance. The proposed DEEP-BTS model achieves a total *AC* of 98.91 % using the dataset. The proposed DEEP-BTS model also achieves overall *SP*, *RE*, *PR*, and *F*1, values of 97.74 %, 97.48 %, 98.24 %, and 96.51 %, respectively.

Table 1. Performance evaluation of the DEEP-BTS.

Types	*AC*	*SP*	*RE*	*PR*	*F*1
CSF	99.12	97.91	97.43	98.76	97.65
GM	98.36	96.75	98.14	97.13	96.14
WM	99.25	98.58	96.87	98.83	95.76
Overall	98.91	97.74	97.48	98.24	96.51

Fig. 5(a) and Fig. 5(b) show the *AC* and loss graphs of the DEEP-BTS model. Fig. 5(a) presents the *AC* curve, with accuracy and epochs on opposing axes; as the number of epochs increases, model *AC* also increases. The epoch versus loss curve in Fig. 5(b) shows that the model's loss decreases as the number of epochs increases. The proposed DEEP-BTS model achieves an *AC* of 98.91 %.

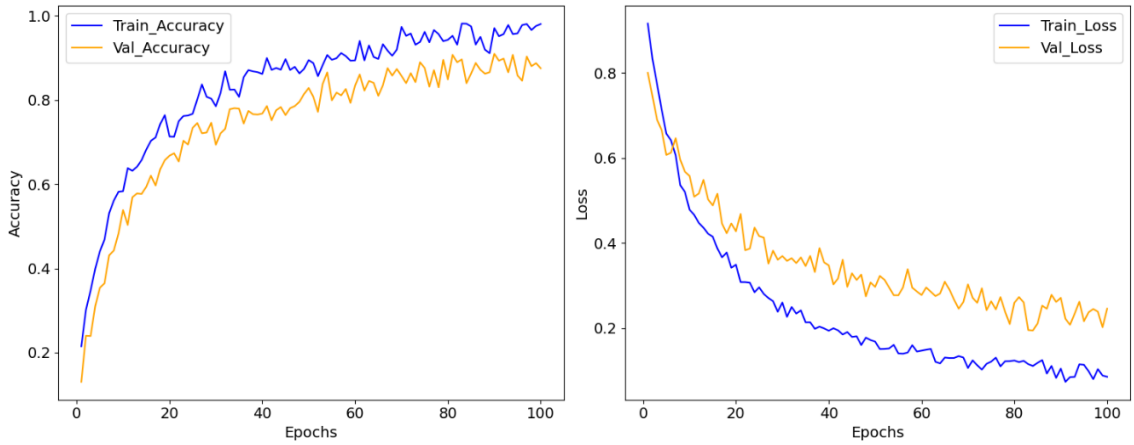

(a) (b)

Fig. 5. (a) Accuracy and (b) Loss curve of the ResU-Net.

B. Comparative analysis

In this section, the experimental results of DEEP-BTS are presented, focusing on a comparison of its performance with other segmentation methods. Fig. 6 offers a summary of the outcomes for Graphcut, SegNet, and U-Net, which are widely used in BTS. Segmentation metrics such as the *JI* and *DI* are used to assess the effectiveness of each algorithm. These metrics help evaluate the precision and accuracy of the segmentation techniques in various scenarios.

Fig. 6 provides a graphical representation of the ResU-Net. It compares various segmentation algorithms with ResU-Net based on *JI* and *DI* metrics. The proposed ResU-Net increases the overall *DI* by 8.63 %, 9.99 %, and 3.07 for Graphcut, SegNet, and U-Net, respectively. According to Table 2, ResU-Net achieves the highest *DI* of 98.50 and *JI* of 97.80 among Graphcut, SegNet, and U-Net algorithms. This analysis indicates that the proposed ResU-Net demonstrates the best segmentation performance.

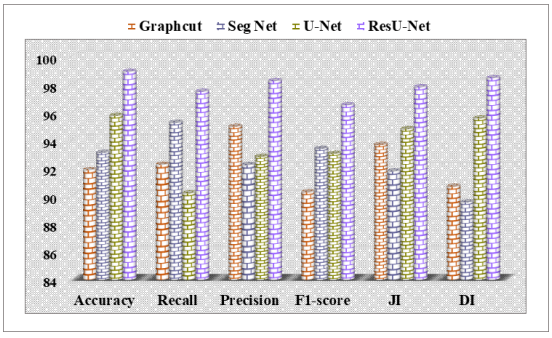

Fig. 6. Comparison of the existing segmentation technique with ResU-Net.

Fig. 7 presents segmentation results for standard U-Net and ResU-Net. Column 1 shows the original input images, and Column 2 shows the ground truth segmentation images from the BrainWeb dataset. Columns 3 and 4 display the segmented results using U-Net and the ResU-Net method, respectively. ResU-Net reduces the false positive rate while improving DEEP-BTS performance. Based on the above comparison, the proposed ResU-Net yields a higher *DI* value than the other segmentation approaches. The segmentation output of ResU-Net is more accurate and closely aligned with the ground truth, capturing fine structural details and boundaries compared to other methods.

Table 2 shows a comparison of existing and proposed models, including Fuzzy C-Means, M-Net, and U-Net. Different segmentation methods yield varying *DI* values for BTS. Fuzzy C-Means [23] achieved *DI* values of 87 % CSF, 89 % GM, and 91 % WM. M-Net [24] produced similar results with 87 % CSF, 89 % GM, and 91 % WM. U-Net [28] performed lower, with 75 % CSF, 79 % GM, and 82 % WM. The proposed ResU-Net outperformed all methods, achieving 98.33 % CSF, 98.04 % GM, and 99.15 % WM, indicating improved segmentation accuracy.

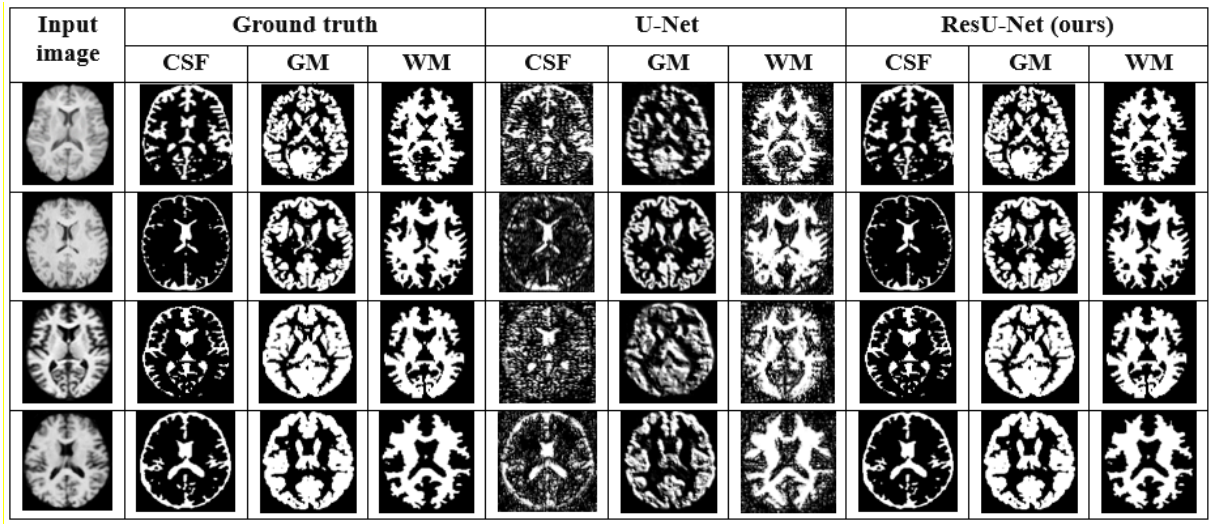

Fig. 7. Segmentation comparison of standard U-Net and the proposed ResU-Net.

Table 2. Comparison of existing methods and DEEP-BTS.

Authors	Techniques	*DI*		
		CSF [%]	GM [%]	WM [%]
Veluchamy, M. and Subramani, B., (2021) [23]	Fuzzy C-Means	87	89	91
Yamanakkanavar, N. and Lee, B., 2020 [24]	M-Net	87	89	91
Srikrishna, M., et al., (2021) [28]	U-Net	75	79	82
Proposed	ResU-Net	98.33	98.04	99.15

Table 3. Performance comparison of the DEEP-BTS model with and without skull stripping and CSATF.

Metrics	without skull stripping without CSATF	with skull stripping without CSATF	with skull stripping with CSATF
AC	97.06	97.88	98.91
*F*1	94.32	95.94	96.51
DI	95.98	97.65	98.50

C. Ablation study

In this analysis, the proposed DEEP-BTS model was evaluated with and without skull stripping and CSATF for BTS.

Table 3 presents the comparative performance of DEEP-BTS under different configurations: with and without skull stripping and CSATF. Without skull stripping and CSATF, the model achieved 97.06 % *AC*, 94.32 % *F*1, and 95.98 % *DI*. Incorporating both skull stripping and CSATF resulted in the highest performance, with 98.91 % *AC*, 96.51 % *F*1, and 98.50 % *DI*. These results clearly indicate that pre-processing steps such as skull stripping and CSATF significantly improve the performance of the DEEP-BTS model in accurately segmenting brain tissues, with the combination of both yielding the most effective outcome.

5. Conclusion

This research introduced a novel DEEP-BTS model for BTS using brain MRI images. The MRI images undergo skull stripping to remove unnecessary regions. The images are denoised by a CSATF to improve image quality, reduce noise artifacts, and for augmentation. The pre-processed images are given to the ResU-Net model, which segments different brain tissues, including CSF, GM, and WM. The proposed ResU-Net increases the overall *DI* by 8.63 %, 9.99 %, and 3.07 % for Graphcut, SegNet, and U-Net, respectively. As a result of the experiment, the proposed method performed 98.91 % more accurately than the previous method in segmenting the classes of brain tissues. The proposed ResU-Net out-performed Fuzzy C-Means, M-Net, and U-Net methods, achieving 98.33 % CSF, 98.04 % GM, and 99.15 % WM, indicating improved segmentation accuracy. Future work in BTS could focus on multi-modal MRI fusion, integrating FLAIR, T1-weighted and T2-weighted images using DL to improve segmentation accuracy, especially for pathological brains.

Acknowledgment

All authors would like to express their heartfelt gratitude to the supervisor for his guidance and unwavering support during this research.

References

[1] Garg, G. (2023). *The Brain Unveiled: Exploring the Wonders of Our Neural World*. Gaurav Garg, ISBN 979-8223672531.

[2] Krishna, K. R., Arbaaz, M., Dhanekula, S. N. C., Vallabhaneni, Y. M. (2024). Modified VGG16 for accurate brain tumor detection in MRI imagery. *Informatyka, Automatyka, Pomiary w Gospodarce i Ochronie Środowiska*, 14 (3), 71-75. http://dx.doi.org/10.35784/iapgos.6035

[3] Raghuram, C., Raju Dandu, V. S. R. K., Jaison, B. (2024). Hybridization of dilated CNN with Attention Link Net for brain cancer classification. *International Journal of Data Science and Artificial Intelligence*, 2 (2), 35-42.

[4] Yuan, Y., Gao, H., Jiang, S., You, Q., Zhou, J., Chen, J. (2025). Magnetic resonance imaging contrast agents based on albumin nanoparticles. *Biomaterials Science*, 13 (2), 408-421. http://dx.doi.org/10.1039/d4bm01226g

[5] Relin Francis Raj, J., Vijayalakshmi, K., Kavi Priya, S., Appathurai, A. (2024). Brain tumor segmentation based on kernel fuzzy c-means and penguin search optimization algorithm. *Signal, Image and Video Processing*, 18 (2), 1793-1802. http://dx.doi.org/10.1007/s11760-023-02849-9

[6] Ahilan, A., Anlin Sahaya Tinu, M., Jasmine Gnana Malar, A., Muthu Kumar, B. (2023). Stationary wavelet-oriented luminance enhancement approach for brain tumor detection with multi-modality images. In *Evolution in Computational Intelligence*. Springer, 461-473. http://dx.doi.org/10.1007/978-981-99-6702-5_38

[7] Anlin Sahaya Infant Tinu, M., Appathurai, A., Muthukumaran, N. (2024). Detection of brain tumour via reversing hexagonal feature pattern for classifying double-modal brain images. *IETE Journal of Research*, 70 (8), 7033-7043. http://dx.doi.org/10.1080/03772063.2023.2301663

[8] Rehman, A., Mir, S. Q. (2025). Introduction to medical image segmentation: Overview of modalities, benchmark datasets, data augmentation techniques, and evaluation metrics. In *Deep Learning Applications in Medical Image Segmentation: Overview, Approaches, and Challenges*. IEEE, 1-26. http://dx.doi.org/10.1002/9781394245369.ch1

[9] Deshpande, A., Estrela, V. V., Jude, A., Hemanth, J. (2025). Computational intelligence in neuroinformatics: Technologies and data analytics. *Neuroscience Informatics*, 5 (1), 100187. http://dx.doi.org/10.1016/j.neuri.2025.100187

[10] Zilioli, A., Rosenberg, A., Mohanty, R., Matton, A., Granberg, T., Hagman, G., Lötjönen, J., Kivipelto, M., Westman, E. (2025). Brain MRI volumetry and atrophy rating scales as predictors of amyloid status and eligibility for anti-amyloid treatment in a real-world memory clinic setting. *Journal of Neurology*, 272 (1), 84. http://dx.doi.org/10.1007/s00415-024-12853-9

[11] Muthukumaran, N., Archana, M., Majitha, A., GiftaIrine, S. T. (2022). Analysis of brain tumor using novel image processing approach. In *2022 3rd International Conference on Electronics and Sustainable Communication Systems (ICESC)*. IEEE, 1387-1393. http://dx.doi.org/10.1109/icesc54411.2022.9885662

[12] Ma, J., He, Y., Li, F., Han, L., You, C., Wang, B. (2024). Segment anything in medical images. *Nature Communications*, 15 (1), 654. http://dx.doi.org/10.1038/s41467-024-44824-z

[13] Chen, X., Sun, S., Bai, N., Han, K., Liu, Q., Yao, S., Tang, H., Zhang, C., Lu, Z., Huang, Q., Zhao, G., Xu, Y., Chen, T., Xie, X., Liu, Y. (2021). A deep learning-based auto-segmentation system for organs-at-risk on whole-body computed tomography images for radiation therapy. *Radiotherapy and Oncology*, 160, 175-184. http://dx.doi.org/10.1016/j.radonc.2021.04.019

[14] Möller, J., Bartsch, A., Lenz, M., Tischoff, I., Krug, R., Welp, H., Hofmann, M. R., Schmieder, K., Miller, D. (2021). Applying machine learning to optical coherence tomography images for automated tissue classification in brain metastases. *International Journal of Computer Assisted Radiology and Surgery*, 16, 1517-1526. http://dx.doi.org/10.1007/s11548-021-02412-2

[15] Nyatega, C. O., Qiang, L., Adamu, M. J., Kawuwa, H. B. (2022). Gray matter, white matter and cerebrospinal fluid abnormalities in Parkinson's disease: A voxel-based morphometry study. *Frontiers in Psychiatry*, 13, 1027907. http://dx.doi.org/10.3389/fpsyt.2022.1027907

[16] Mahmood, T., Rehman, A., Saba, T., Nadeem, L., Bahaj, S. A. O. (2023). Recent advancements and future prospects in active deep learning for medical image segmentation and classification. *IEEE Access*, 11, 113623-113652. http://dx.doi.org/10.1109/access.2023.3313977

[17] Xu, Y., Quan, R., Xu, W., Huang, Y., Chen, X., Liu, F. (2024). Advances in medical image segmentation: A comprehensive review of traditional, deep learning and hybrid approaches. *Bioengineering*, 11 (10), 1034. http://dx.doi.org/10.3390/bioengineering11101034

[18] Richter, L., Fetit, A. E. (2022). Accurate segmentation of neonatal brain MRI with deep learning. *Frontiers in Neuroinformatics*, 16, 1006532. http://dx.doi.org/10.3389/fninf.2022.1006532

[19] Mohammadi, Z., Aghaei, A., Moghaddam, M. E. (2024). CycleFormer: Brain tissue segmentation in the presence of Multiple Sclerosis lesions and Intensity Non-Uniformity artifact. *Biomedical Signal Processing and Control*, 93, 106153. http://dx.doi.org/10.1016/j.bspc.2024.106153

[20] Kollem, S. (2024). An efficient method for MRI brain tumor tissue segmentation and classification using an optimized support vector machine. *Multimedia Tools and Applications*, 83, 68487-68519. http://dx.doi.org/10.1007/s11042-024-18233-9

[21] Gudise, S., Giri Babu, K., Satya Savithri, T. (2024). An advanced fuzzy C-Means algorithm for the tissue segmentation from brain magnetic resonance images in the presence of noise and intensity inhomogeneity. *The Imaging Science Journal*, 72 (4), 520-539. http://dx.doi.org/10.1080/13682199.2023.2210400

[22] Daoudi, A., Mahmoudi, S. (2024). Enhancing brain segmentation in MRI through integration of hidden markov random field model and whale optimization algorithm. *Computers*, 13 (5), 124. http://dx.doi.org/10.3390/computers13050124

[23] Veluchamy, M., Subramani, B. (2021). Brain tissue segmentation for medical decision support systems. *Journal of Ambient Intelligence and Humanized Computing*, 12 (2), 1851-1868. http://dx.doi.org/10.1007/s12652-020-02257-8

[24] Yamanakkanavar, N., Lee, B. (2020). Using a patch-wise M-net convolutional neural network for tissue segmentation in brain MRI images. *IEEE Access*, 8, 120946-120958. http://dx.doi.org/10.1109/access.2020.3006317

[25] Long, J.-S., Ma, G.-Z., Song, E.-M., Jin, R.-C. (2021). Learning U-net based multi-scale features in encoding-decoding for MR image brain tissue segmentation. *Sensors*, 21 (9), 3232. http://dx.doi.org/10.3390/s21093232

[26] Karimi, D., Rollins, C. K., Velasco-Annis, C., Ouaalam, A., Gholipour, A. (2023). Learning to segment fetal brain tissue from noisy annotations. *Medical Image Analysis*, 85, 102731. http://dx.doi.org/10.1016/j.media.2022.102731

[27] Qi, W., Wei, M., Yang, W., Xu, C., Ma, C. (2020). Automatic mapping of landslides by the ResU-Net. *Remote Sensing*, 12 (15), 2487. http://dx.doi.org/10.3390/rs12152487

[28] Srikrishna, M., Pereira, J. B., Heckemann, R. A., Volpe, G., van Westen, D., Zettergren, A., Kern, S., Wahlund, L.-O., Westman, E., Skoog, I., Schöll, M. (2021). Deep learning from MRI-derived labels enables automatic brain tissue classification on human brain CT. *Neuroimage*, 244, 118606. http://dx.doi.org/10.1016/j.neuroimage.2021.118606

Received February 21, 2025
Accepted September 8, 2025